The British Journal of Radiology, 85 (2012), e1009–e1017

In vivo 3 T MR diffusion tensor imaging for detection of the fibre architecture of the human uterus: a feasibility and quantitative study

[1]F FIOCCHI, MD, [2]L NOCETTI, MS, [1]E SIOPIS, MD, [1]S CURRÀ, MD, [2]T COSTI, MS, [1]G LIGABUE, MD and [1]P TORRICELLI, MD

[1]*Department of Diagnostic Radiology, Policlinico Hospital, University of Modena and Reggio-Emilia, Modena, Italy, and* [2]*Department of Physics, Policlinico Hospital, University of Modena and Reggio-Emilia, Modena, Italy*

Objective: The aim of this study was to investigate the feasibility of depicting fibre architecture of human uteri *in vivo* using 3 T MR diffusion tensor imaging (MR-DTI) with a three-dimensional (3D) tractography approach. Quantitative results were provided.

Methods: *In vivo* 3 T MR-DTI was performed on 30 volunteers (9 Caesarean delivery). Main diffusion directions reflecting the fibre orientation were determined using sensitivity-encoding single-shot echo planar imaging with diffusion-sensitised gradients (b=600 mm^2 s^{-1}) along 32 directions. A deterministic fibre-tracking algorithm was used to show *in vivo* fibre architecture, compared with *ex vivo* histological slides of cadaveric uteri. The number of fibres, the fibre density, the fractional anisotropy (FA) and the apparent diffusion coefficient (ADC) were measured in 13 volunteers.

Results: Anisotropy was found in most regions of normal uteri and the preferential order of uterine fibres depicted, consisting of two representative fibre directions: circular and longitudinal, as in *ex vivo* studies. Two-thirds of uteri with a Caesarean scar did not have the same orientation of fibres in the anterior isthmus when compared with non-scarred myometrium. Quantitative data were obtained from 13 volunteers: Caesarean-scarred uteri (n=5) showed lower fibre number and density in the scarred anterior isthmus than the nulliparous uteri (n=8). No significant differences were found in FA (0.42 ± 0.02, 0.41 ± 0.02; p=0.25) and ADC ($1.82 \pm 0.18 \times 10^{-3}$ mm^2 s^{-1}, $1.93 \pm 0.25 \times 10^{-3}$ mm^2 s^{-1}; p=0.20).

Conclusion: Fibre architecture of the human uterus can be depicted *in vivo* using 3 T MR-DTI.

Advances in knowledge: 3 T MR-DTI can help to provide an *in vivo* insight of uterine anatomy non-invasively, especially in females with previous Caesarean surgery, in order to provide better management of subsequent deliveries.

Received 16 December 2011
Revised 9 March 2012
Accepted 29 March 2012

DOI: 10.1259/bjr/76693739

The human uterus is a fibromuscular organ composed of three layers: the endometrium (the innermost mucosal layer, lining the uterine cavity), the myometrium (the middle layer, consisting of smooth muscle bundles and connective tissue) and the perimetrium (the outer layer, corresponding to the peritoneum). The overall arrangement of muscle fibres in the human uterus has been extensively investigated [1], showing that the uterine wall consists of two counter-rotating systems of spiral fibres. Fibres in the myometrium are divided into the internal layer (stratum subvascolare), which mostly run in a circular pattern, and the external layer (stratum supravascolare), which mostly run in a longitudinal pattern. There is also an intermediate layer (stratum vascolare) in which the fibres run in random directions.

Address correspondence to: Dr Federica Fiocchi, Policlinico Hospital, University of Modena and Reggio-Emilia Department of Diagnostic Radiology, Via del Pozzo 71, 41124 Modena, Italy. E-mail: federica.fiocchi@gmail.com

Research has led to constant advancements in MR hardware and software. One such example is the evolution of diffusion tensor imaging from diffusion-weighted imaging [2, 3]. MR diffusion tensor imaging (MR-DTI) is an emerging non-invasive method to determine the amount of random diffusion (Brownian motion) of water molecules in tissues, providing physiological information about the mobility of water that aids in tissue characterisation. The technique works by assuming water molecules will diffuse in the same direction as the general orientation of the fibres rather than perpendicular to them. Anisotropy can be quantified by calculating the diffusion tensor, which depicts the preferential water movement using multiple diffusion-weighted acquisitions with directionally varying diffusion sensitisation gradients. Another recent advancement is in the collaborative use of MR-DTI and fibre tractography. Fibre tractography is a novel software application that estimates the tensor value of each voxel to obtain the direction of fibres in a three-dimensional

(3D) image, starting from the water diffusion profile in each voxel. It works by depicting the intervoxel connectivity based on the anisotropic diffusion of water to give quantitative information on the dominant direction of the water in a well-organised tissue.

The MR-DTI with 3D fibre tractography approach has been successfully applied to the analysis of neuronal pathways in the brain *in vivo* [4], but there are few studies that do not concern neuronal applications. There have been several MR-DTI feasibility studies in animals showing the anatomical fibre distribution in skeletal muscle, tongue and heart [5–7]. There have also been some studies on *in vivo* human skeletal muscle [8, 9], tongue [10] and ventricular myocardium [11]. There is only one study on the uterus using MR-DTI, which was performed *ex vivo* on patients subjected to a hysterectomy for medical reasons [12]. They demonstrated that uterine muscle fibre direction or anisotropy can be estimated because water molecules diffuse more easily along the muscle fibres than across them, highlighting the extremely structured muscular tissue. The method was validated against histological slides and depicted two systems of fibres running circularly along the intramural part of the uterine tubes, indicating that MR-DTI is a beneficial and complementary tool to standard microscopic techniques to determine the intrinsic fibre architecture [12].

We hypothesise that if such a well-organised structure is in any way altered, for example by Caesarean surgery, the fibre architecture will show some degree of disarray.

Caesarean deliveries are still increasing in Western society, often due to medicolegal reasons [13]. The incidence of placenta previa and/or placenta accrete in females with previous Caesarean section is much higher than in females with normal deliveries. As a consequence, there has also been a rise in the number of abnormal placental insertions, which are the major causes of mortality or hysterectomy due to post-partum haemorrhage complications [14, 15]. This suggests that the structural architecture of the uterus altered by Caesarean surgery could predispose the development of placental abnormalities in subsequent pregnancies.

The first purpose of the study was to verify the feasibility of using a 3 T MR-DTI with a 3D tractography approach in depicting fibre architecture of the uterus *in vivo*. The secondary aim was to compare the fibre architecture of non-scarred uteri with Caesarean-scarred uteri *in vivo*. Furthermore, preliminary data using 3 T MR-DTI are shown regarding the number of fibres, the fibre density, the fractional anisotropy (FA) and the apparent diffusion coefficient (ADC).

Methods and materials

Patient population

From April 2009 to October 2010, 30 volunteers (mean age 36.3 ± 11.7 years old; 13.3% post-menopausal) were enrolled. The procedures followed were approved by the local ethics committee and in accordance with the ethical standards of the responsible committee on human experimentation at the Helsinki Declaration of 1975. All volunteers gave written informed consent.

Exclusion criteria were general contraindication to MR examination, pregnancy and uterine leiomyomas.

Of the 30 volunteers, 14 patients had no previous pregnancy, 16 patients had previous pregnancy with 7 vaginal deliveries (5 patients had 1 previous delivery and 2 patients had 2 previous deliveries) and 9 patients with a Caesarean section (3 patients had 2 previous Caesarean sections and 6 patients had 1 Caesarean section). Two of the patients who had undergone Caesarean surgery had positive anamnesis for placenta previa and placenta previa accrete during their second pregnancy.

MR-DTI uterine morphological results were compared with three *ex vivo* uteri, of which two were cadaveric (one female with no previous delivery and one female with previous vaginal delivery) and one uterus with prior Caesarean deliveries excised due to *in situ* cervical carcinoma (2 μm haematoxylin and eosin macrosection). The last one was previously studied with MR-DTI.

The patient characteristics are reported in Table 1.

MR technique

All patients underwent 3 T MRI (Achieva, Philips Medical Systems, Best, Netherlands) using a six-channel coil phased-array Synergy-Cardio (Philips Medical Systems) in the supine position. The maximum gradient strength was 40 mT m^{-1}, and the maximum slew rate was 200 $Tm^{-1}s^{-1}$. The study protocol included preliminary morphological spin-echo (SE) sequences on the female pelvis (from the renal hila to the pubic symphysis) considering the uterus's long and short axis and three fast sequences [single-shot turbo SE (Ssh-TSE)] on the uterus's long and short axes in order to plan a diffusion-weighted sequence in multiple directions used for DTI imaging.

All volunteers were asked to fast from midnight in order not to have significant differences in body temperature. In four cases, the bladder was too full, and this caused minimal artefacts in post-processing of DTI imaging.

20 mg of butyl-scopolamine (Buscopan; Schering, Ingelheim, Germany) was administered intravenously to all volunteers before examination to prevent peristalsis artefacts.

Sequence parameters were as follows:

- axial T_1 weighted SE: echo time (TE) 10 ms, repetition time (TR) 600 ms, field of view (FOV) 21×21 cm, matrix 256×256, thickness 4 mm, gap 1 mm, number of signal acquisition (NSA) 2
- sagittal T_2 weighted SE on the long axis of the uterus: TE 80 ms, TR 5000 ms, FOV 21×21 cm, matrix 256×256, thickness 4 mm, gap 1 mm, NSA 3
- coronal T_2 weighted SE on the uterus short axis: TE 80 ms, TR 4000 ms, FOV 21×21 cm, matrix 256×256, thickness 4 mm, gap 1 mm, NSA 3
- axial, sagittal and parasagittal T_2 weighted Ssh-TSE: TE 80 ms, TR 1300 ms, FOV $35 \times 25 \times 15$ cm, matrix 300×175, thickness 5 mm, NSA 1, sensitivity encoding 2. The parasagittal sequence is acquired with the sagittal plane of the body rotated on the long axis of the uterus.

Table 1. Patients' characteristics

Volunteer	Age (years)	Menstrual cycle	Deliveries	Caesarean delivery	Placenta at second pregnancy
1	30	Luteal phase	–	–	–
2	28	Luteal phase	–	–	–
3	29	Luteal phase	–	–	–
4	29	Menses	–	–	–
5	27	Luteal phase	–	–	–
6	29	Luteal phase	–	–	–
7	28	Luteal phase	–	–	–
8	29	Luteal phase	–	–	–
9	30	Luteal phase	P2 D2	2	Normal
10	*34*	Luteal phase	P2 D2	2	*Previa accrete*
11	*29*	Luteal phase	P2 D2	2	*Previa*
12	55	Luteal phase	P2 D2	–	
13	73	Luteal phase	P1 D1	1	Normal
14	29	Luteal phase	–	–	–
15	26	Menses	–	–	–
16	36	Luteal phase	P1 D1	1	Normal
17	47	Luteal phase	P1 D1	1	Normal
18	35	Luteal phase	P2 D2	–	Normal
19	30	Follicular phase	P1 D1	–	Normal
20	31	Luteal phase	P1 D1	–	Normal
21	32	Follicular phase	P1 D1	–	Normal
22	32	Follicular phase	–	–	–
23	25	Luteal phase	–	–	–
24	27	Luteal phase	–	–	–
25	44	Menses	–	–	–
26	47	Menses	P1 D1	1	Normal
27	55	Menopause	P1 D1	1	Normal
28	59	Menopause	P1 D1	–	–
29	42	Menopause	P1 D1	1	–
30	41	Menopause	P1 D1	–	–

P, pregnancy; D, deliveries.
Volunteers number 10 and 11 written in italics are the ones with placental complication at second delivery.

The diffusion-weighted sequence is a fast echo planar sequence [Ssh-echo planar imaging (EPI)] where multiple echoes are acquired, so that artefacts from movement are minimised [7]. Uterine contractions and intestinal peristalsis can cause artefacts that disturb image acquisition and invalidate the results. Diffusion-weighted Ssh-EPI was acquired with spectral fat saturation and half-Fourier sampling along 32 directions to obtain DTI. Sequences were obtained with $b=600\,\mathrm{mm^2\,s^{-1}}$.

Diffusion-weighted Ssh-EPI was performed on the parasagittal plane with the following parameters: TE 70 ms, TR >5000 ms, FOV $31\times31\times84$ cm, matrix 140×140, thickness 2.1 mm, NSA 2, clear yes, EPI factor 135, fold over anteroposterior, $b=600\,\mathrm{mm^2\,s^{-1}}$, scan time along 32 directions 5 min 27 s.

Image analysis

Diffusion-weighted Ssh-EPI images are processed on a dedicated workstation for data pre-processing with MedINRIA software (MedINRIA v. 2.0, Medical Image Navigation and Research tool by Sophia Antipolis, Research project ASCLEPIOS). Diffusion eigenvalues and eigenvectors were estimated in each voxel in order to calculate the FA and ADC maps; and then with a proper tool (deterministic DTI.Track; MedINRIA v. 2.0) fibre tracking is performed. Tracking is continued until the stop criteria are satisfied. To help fibre visualisation in the final fibre tracking, a minimal FA of 0.2 and a maximal angle change of 10° per integration step were used. Fibres underlining the preferential water movement used a reference vector colour-coded map (assigning red, green and blue to each orthogonal direction). Within 5–10 min all fibres were appreciable, but if fibres of all the voxels that determine the uterus are used in this fashion, it results in no visible structures. In reliance on the numbers, the dimension and the localisation of different regions of interest (ROIs) drawn, it is possible to obtain simple to complex structures with different degrees of reading. Therefore a reduction in fibre is used to reveal first the global uterus architecture and second specific fibre orientation and distribution, in order to identify longitudinal or circular fibres, different ROIs were placed on the uterus, particularly on the isthmus (Figure 1).

3 T MR-DTI fibre tractography can provide not only morphological reconstruction but also quantitative results can be extrapolated. Data were obtained regarding the number of fibres, the fibre density, the FA and the ADC in 13 patients, of whom 8 had no previous pregnancy (Group I) and 5 had a previous Caesarean delivery (Group II). Data from these 13 patients were analysed to find differences in fibre architecture between non-scarred uteri and Caesarean-scarred uteri.

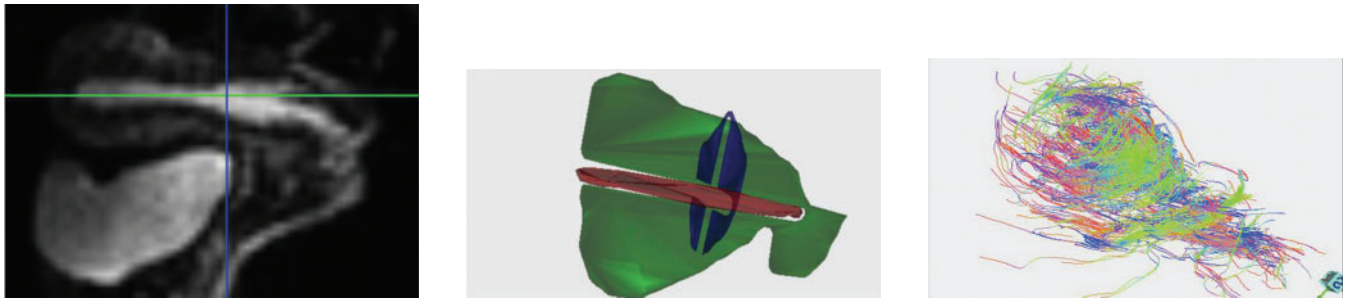

(a) (b) (c)

Figure 1. Volunteer number 3, 29 years old. Example of whole-uterus diffusion tensor imaging (DTI) fibre tracking representation. Regions of interest [sagittal view (a)] are drawn to depict fibres of the whole uterus (b). (c) Fibre tracking after processing results in global uterus fibre architecture.

Statistical analysis

The *t*-test was performed to assess statistical significance of differences in the fibre's density, FA and ADC values between the non-pregnancy group and Caesarean section group.

Results

Uterine fibre anisotropy was confirmed by 3 T MR-DTI image reconstruction in volunteers with no previous pregnancies: the uterine muscular structure was shown to be a highly arranged tissue, characterised by organised fibre architecture, composed of smooth muscle cells and collagen fibre, which was the basis for the preferential direction of movement of water molecules. None of the volunteers had any complications during 3 T MRI-DTI examination.

For 3 T MR-DTI morphological analysis, fibre tracking of the global uterine structure and the inferior uterine segment were feasible in all but one case. The mean 3 T MR-DTI processing time was 1 h $\pm$ 14 min. In one patient, the 3 T MR-DTI morphological results were difficult to extrapolate because of a tube ligature after Caesarean delivery; it took significantly longer to reconstruct the image for this patient (2 h and 18 min).

Bladder overdistension caused some artefacts in fibre reconstruction, since it led to an increase in background noise. This phenomenon was seen in the first volunteer, and all subsequent patients were instructed to empty their bladder before the scan.

Uterine fibres in the 21 volunteers with non-scarred uteri showed the architecture previously described in the literature [1] with the internal circular layer (stratum subvascolare) (Figure 2) and the external longitudinal layer (stratum supravascolare) (Figure 3) clearly seen. These two fibre bundles are closely related to one another so it was sometimes hard to visualise the layers separately using DTI reconstruction, even when specific ROIs were drawn in order to depict selected directions.

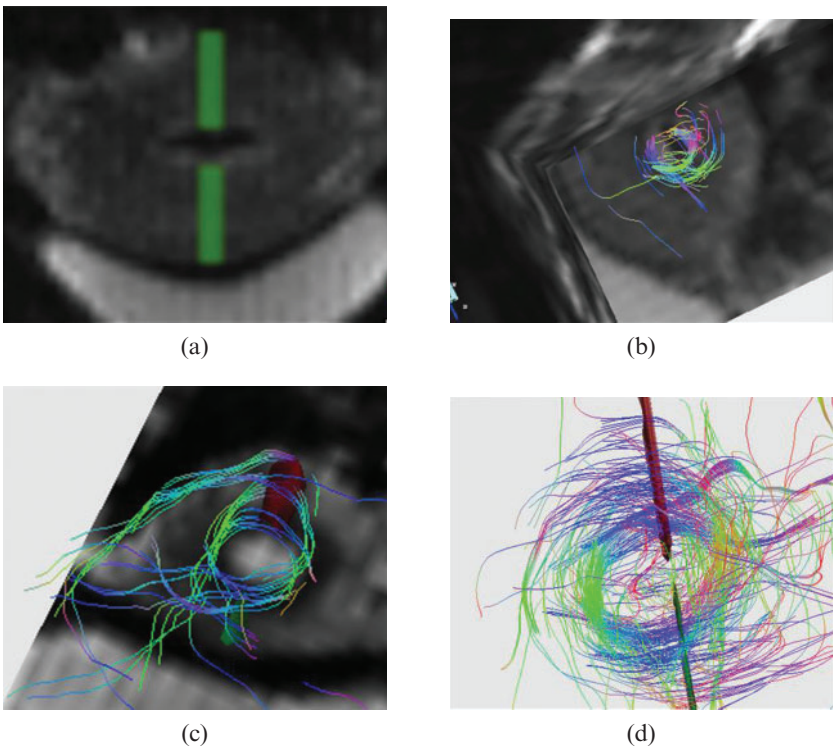

(a) (b) (c) (d)

Figure 2. Volunteer number 22, 32 years old. On uterus short-axis diffusion tensor imaging (a) two symmetrical regions of interest (ROIs) are drawn in order to depict inner circular layer as visible on three-dimensional reconstruction (b). Volunteer number 23, 25 years old. Specific ROIs are drawn in order to depict inner circular fibre bundle appreciable both in superimposed diffusion tensor imaging post-processed image (c) and on fibre tracking results alone (d).

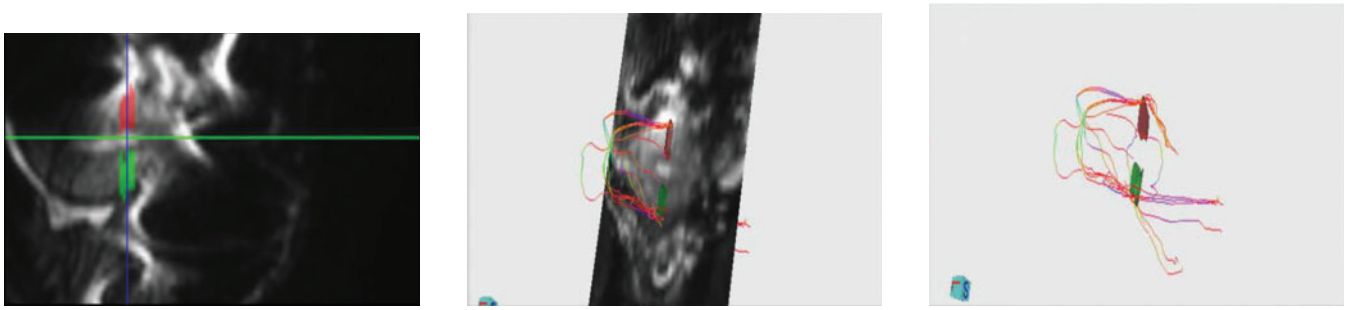

(a) (b) (c)

Figure 3. Volunteer number 1, 30 years old. On uterus vertical long-axis diffusion tensor imaging (DTI) image (a) two symmetrical regions of interest are drawn in order to depict an external longitudinal layer appreciable both in superimposed DTI post-processed image (b) and on fibre tracking results alone (c).

Histological specimens of the *ex vivo* uteri show the actual fibre architecture; the 3 T MR-DTI image reconstruction was similar to the corresponding histological stains showing normal fibre direction (Figure 4). The comparison between the *in vivo* 3 T MR-DTI reconstruction of a volunteer with a Caesarean-scarred uterus subsequently removed due to cervical carcinoma showed morphological correlation (Figure 4), with a reduction in myometrium thickness, altered fibre architecture and irregular fibre direction in the endometrium.

We did not find differences in fibre architecture between the nulliparous volunteers and those with previous vaginal pregnancy, except for the overall uterine dimensions, which were larger and a more triangular uterine cavity in the latter group.

Regarding females with a record of Caesarean delivery, the damage created by hysterectomy suture in the anteroinferior segment was appreciable in the morphological sequences as well as in the subsequent 3 T MR-DTI reconstruction. Within the volunteers with a previous Caesarean section there were clear differences between the three patients with a ''clear'' surgery and the six patients with a ''rough'' surgery. DTI fibre tracking shows disrupted bundle architecture (Figure 5) with interrupted fibre directions throughout the suture in the Caesarean uteri with rough surgery, whereas in Caesarean uteri with clear surgery fibre directions can still depicted (Figure 6). Furthermore, the two volunteers with the most altered fibre structure depicted by 3 T MR morphological and DTI reconstruction images went on to have placental abnormalities (one placenta previa and one placenta accrete) during their subsequent pregnancy.

Preliminary data from 13 volunteers were obtained using 3 T MR-DTI reconstruction for the fibre number, the fibre density, the FA and the ADC. Several different ROIs were used on the whole uterine volume, the anterior isthmus segment and the anterior and posterior uterine wall. Volunteers 1–8 had no previous delivery (Group I), whereas volunteers 9–13 had had Caesarean surgery (Group II).

Regarding the whole uterine structure (Table 2) we did not find significant differences between the two volunteers groups. The mean fibre density (number of fibres cm^{-3}) was similar between the two groups (380 ± 120 in Group I and 340 ± 60 in Group II; $p=0.25$) as well as FA (0.41 ± 0.02 and 0.42 ± 0.02; $p=0.25$).

The mean ADC was a little bit higher in Group I ($1.93 \pm 0.25 \times 10^{-3}$ mm^2 s^{-1}) than in Group II ($1.82 \pm 0.18 \times 10^{-3}$ mm^2 s^{-1}), although this was not statistically significant ($p=0.20$). A possible explanation for these results is the small number of volunteers studied.

Moreover, we analysed the results of drawing an ROI of the same dimension on the anterior isthmus segment and the posterior and anterior uterine wall. Volunteers 1–8 had no previous deliveries (Group I), whereas volunteers 9–13 had Caesarean surgery (Group II). The mean fibre number and density (number of fibres mm^{-3}) in the anterior isthmus segment was higher in Group I than in Group II: 110 ± 50 *vs* 80 ± 50 and 4.5 ± 2.1 *vs* 3.2 ± 2.0, respectively. The mean ADC was a little bit higher in Group I ($1.9 \pm 0.4 \times 10^{-3}$ mm^2 s^{-1}) than in Group II ($1.8 \pm 0.2 \times 10^{-3}$ mm^2 s^{-1}), although again this was not statistically significant. Group II could be further divided into two subgroups of volunteers with no placental abnormalities at subsequent delivery (Subgroup IIa, volunteers 9, 12 and 13) and volunteers with placenta previa and placenta previa accrete during their subsequent pregnancy (Subgroup IIb, volunteers 10 and 11). Comparing the two subgroups we found that volunteers who developed placental abnormalities (Subgroup IIb) had the scars with the most fibre disruption on morphological analysis and had the lowest quantitative data, in particular a lower mean fibre number and density than subgroup IIa (34 ± 12 and 2.1 ± 0.4 *vs* 105 ± 33 and 9.7 ± 1.03, respectively) and a lower mean ADC ($1.67 \pm 0.02 \times 10^{-3}$ mm^2 s^{-1} *vs* $1.92 \pm 0.2 \times 10^{-3}$ mm^2 s^{-1}). Results are reported in Table 3.

Discussion

In this study we were able to depict the global fibre architecture of the human uterine myometrium *in vivo* using 3 T MR-DTI. The representation of the fibre architecture seen appears accurate, as anisotropy was found throughout the non-scarred uteri in an almost identical pattern to that shown previously by an *ex vivo* study [12], histological staining and anatomical reports. There is always a concern with the accuracy of new imaging techniques, especially those looking at detailed anatomical definition *in vivo*. This is even more of a concern with 3 T MR-DTI imaging as only the general

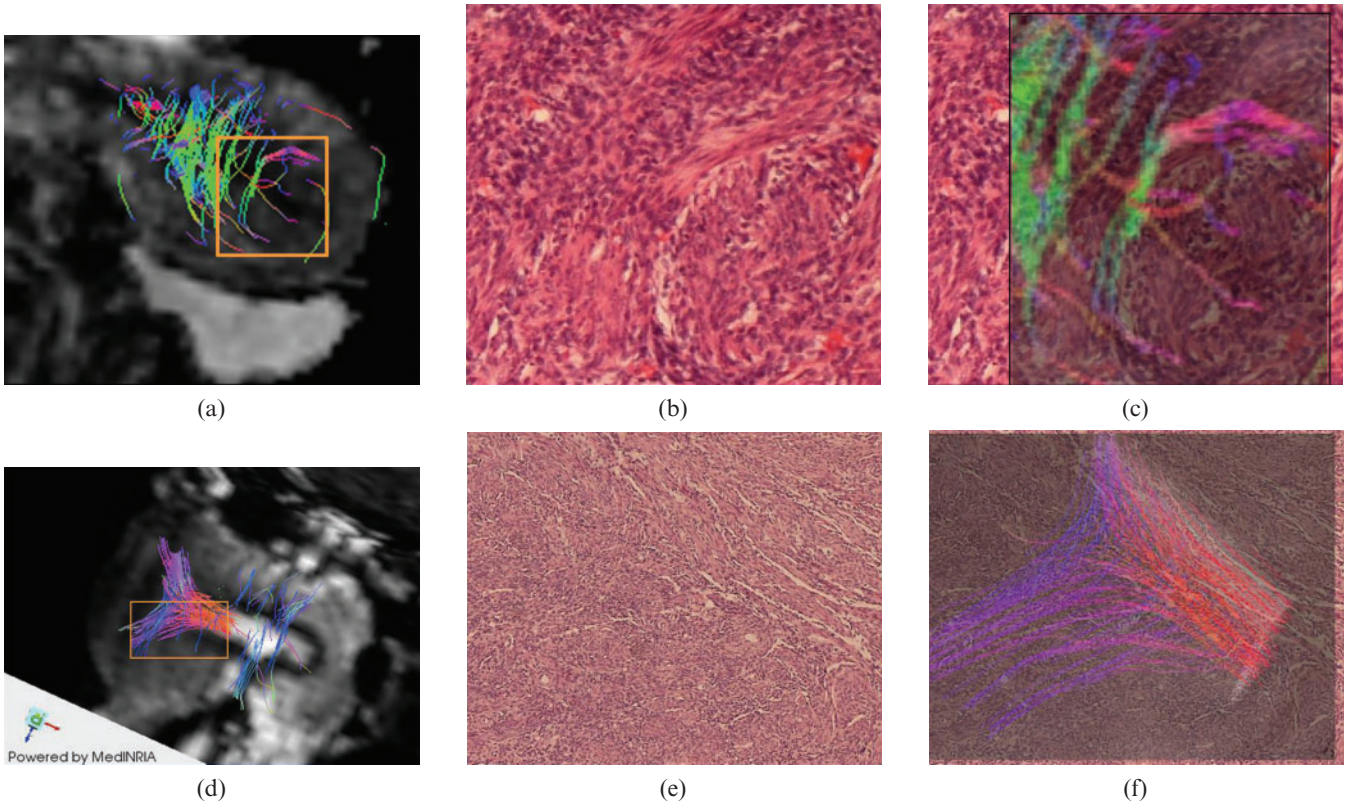

Figure 4. 3 T MR-diffusion tensor imaging (DTI) reconstruction was compared with the corresponding histological specimens of the *ex vivo* uteri that accurately show similar fibre architecture for both circular (first row) and longitudinal (second row) fibre bundle. (a) Circular fibre bundle superimposed to DTI post-processed image. (b,c) Histological specimen (haematoxylin and eosin) without and with circular fibre superimposition. (d) Longitudinal fibre bundle superimposed to DTI post-processed image. (e,f) Histological specimen (haematoxylin and eosin) without and with circular fibre superimposition.

direction of the muscle fibres can be depicted. Each voxel within the image contains a large number of fibres that are orientated in different directions, but the software processes the information to show the average fibre direction and assumes that collagen and muscle fibres must have the same main organisation. Another issue arises when determining the fibre orientation in the circular layer of the myometrium, as artefacts can be caused by the presence of air in the uterine cavity and by constant small movements due to breathing and/or spontaneous uterine contractions. Moreover a limitation could be the use of modified software used in functional neurology to process the data, since dedicated software designed for uterine muscle architecture is not available. Dedicated software could significantly enhance the images. However, these limitations were overcome as the *in vivo* 3 T MR-DTI fibre tracking was comparable with the main fibre directions depicted in *ex vivo* histological analysis.

There are only a select few quantitative DTI analyses carried out on *in vivo* human tissue such as the muscles in the thigh and the median nerve [9, 16]. These studies have shown that it is possible to obtain the 3D architecture and microstructural parameters such as FA

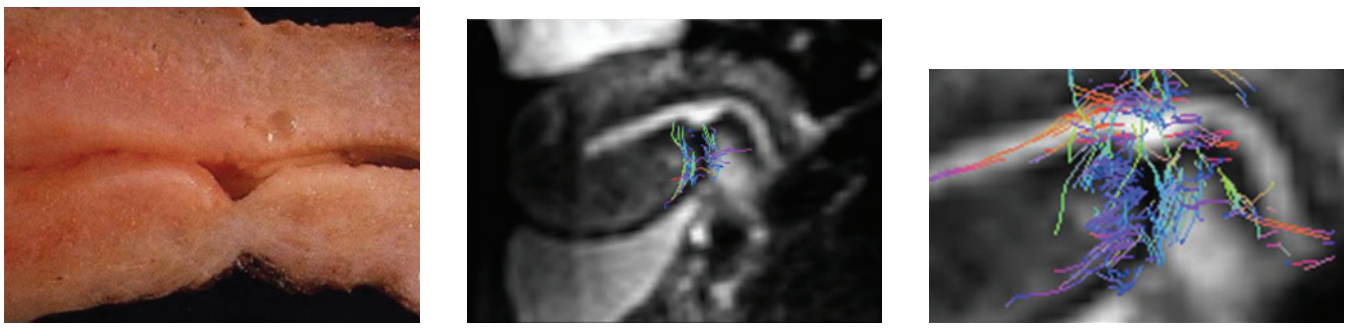

Figure 5. Volunteer number 10, 34 years old, with two Caesarean deliveries. This volunteer was then submitted to hysterectomy because of an *in situ* cervical carcinoma. (a) Macroscopic sagittal cut of the uterus at scar level. (b) 3 T MR-diffusion tensor imaging (DTI) showing concordance with the *ex vivo* anatomy. (c) Fibre bundle superimposed to DTI post-processed image that shows interruption and disarray at scar level.

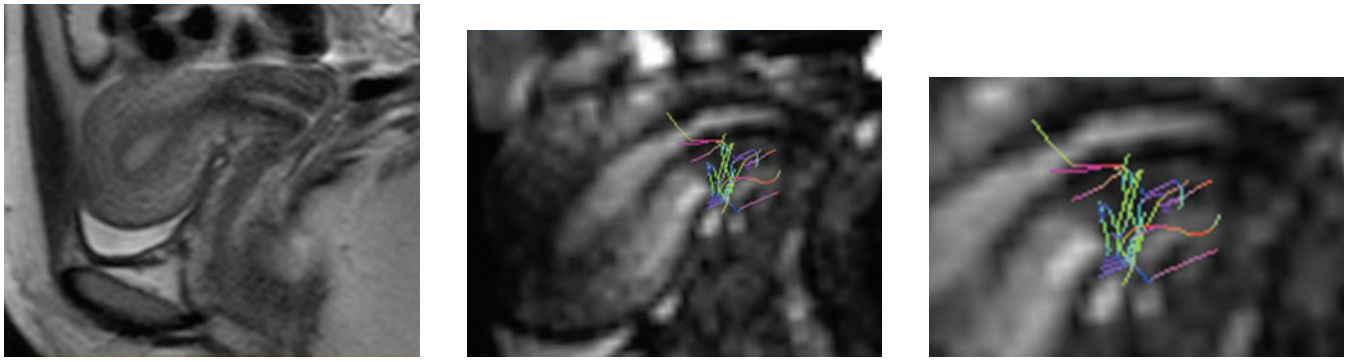

(a) (b) (c)

Figure 6. Volunteers number 9, 30 years old with Caesarean delivery. (a) Sagittal T_2 spin-echo sequence showing the absence of significant disruption of the anterior uterine wall where the Caesarean suture is poorly visible. (b) 3 T MR-diffusion tensor imaging post-processed image with superimposed fibre bundle shows that the circular bundle is still present and also some longitudinal fibres are depicted, especially in the zoomed view (c).

and ADC using 3 T MR-DTI. In the present study we were also able to obtain quantitative data from a selected number of volunteers. Unexpectedly, we found there were no significant differences in the FA and ADC values between the scarred and non-scarred uteri when analysing the whole uterus. Upon closer inspection of the ADC value for both groups, there was a reasonable difference, with the non-scarred uteri having an ADC value of $1.93 \pm 0.25 \times 10^{-3}$ mm^2 s^{-1} and Caesarean-scarred uteri having an ADC value of $1.82 \pm 0.18 \times 10^{-3}$ mm^2 s^{-1}. The fact that this was not significant may be explained by the small population of volunteers studied. We would have expected the ADC value to be significantly different between the two groups, because Caesarean surgery would disrupt the fibre architecture preventing anisotropic water movement along the muscle fibres. In order to obtain more reliable quantitative data, a study with a larger population is in progress.

3 T MR-DTI imaging of Caesarean-scarred uteri showed that the previous surgery in the anterior isthmus segment caused fibre disruption. Within the scarred tissue of the uteri there was a varying degree of muscle fibre disruption. The two volunteers with the greatest fibre disruption and the lowest number of fibres within the anterior isthmus region (Group IIb) both developed placenta previa or placenta previa accrete during their subsequent pregnancies. It is likely that the amount of disruption to the fibre orientation and the loss of fibres caused by surgery are associated with placental mal-insertions in future deliveries [14, 15]. Caesarean deliveries are progressively more common in developed countries; in the last available report they increased from 31.8% in 2007 to 32.3% in 2008 [13]. As a result, more placental abnormalities are now occurring, leading to higher mortality rates and more hysterectomies due to major uterine haemorrhage [17, 18]. We hope that in future the added information provided by 3 T MR-DTI of a Caesarean-scarred uterus will highlight which females have a high risk of placental complications. This added information could change the management of subsequent pregnancies when it comes to choices such as closer observation throughout the pregnancy, best modality of delivery and planned conservative therapies, such as uterine artery embolisation to prevent a hysterectomy. Moreover, MRI-DTI can be used to find

Table 2. Fibre number, density, FA and ADC posing different regions of interest on whole uterine volume

Volunteers	Number	Mean FA	Mean ADC (10^{-3} mm^2 s^{-1})	Density (n fibres cm^{-3})
1	18 559	0.41	2.17	532.70
2	24 377	0.42	2.12	291.86
3	14 056	0.38	2.21	389.15
4	18 923	0.38	2.09	431.70
5	7531	0.42	1.71	544.33
6	13 509	0.44	1.54	370.55
7	23 097	0.39	1.90	212.39
8	12 811	0.40	1.72	304.88
Mean $\pm$ SD	16 600 $\pm$ 5700	0.41 $\pm$ 0.02	1.93 $\pm$ 0.25	380 $\pm$ 120
9	14 528	0.42	1.68	372.34
10	*17 389*	*0.42*	*1.76*	*323.71*
11	*19 054*	*0.44*	*1.64*	*379.71*
12	23 279	0.40	1.96	240.53
13	22 958	0.39	2.05	400.44
Mean $\pm$ SD	17 400 $\pm$ 3700	0.42 $\pm$ 0.02	1.82 $\pm$ 0.18	340 $\pm$ 60

ADC, apparent diffusion coefficient; FA, fractional anisotropy; SD, standard deviation.
Volunteers number 10 and 11 written in italics are the ones with placental complication at second delivery.

Table 3. Fibre number, density (*n* fibres mm^{-3}), FA and ADC posing different regions of interest anterior isthmus segment, posterior and anterior uterine wall

	Anterior isthmus segment				Posterior uterine wall		Anterior uterine wall	
Volunteers	Number	Density	Mean FA	Mean ADC	Number	Density	Number	Density
1	74	2.51	0.37	2.22	30	0.81	36	1.22
2	113	5.78	0.42	1.99	111	3.41	91	3.49
3	139	7.11	0.36	2.61	94	3.61	50	1.92
4	148	5.68	0.4	1.74	61	3.12	79	3.03
5	17	2.30	0.39	1.74	12	1.63	15	1.02
6	90	3.05	0.43	1.50	106	7.18	85	2.88
7	105	2.37	0.37	2.01	143	1.94	258	3.49
8	160	6.77	0.41	1.64	33	1.75	54	2.86
Mean ± SD	110 ± 50	4.5 ± 2.1	0.38 ± 0.03	1.9 ± 0.4	70 ± 50	2.9 ± 2.0	80 ± 70	2.5 ± 1.0
9	97	4.38	0.38	1.73	86	2.33	46	1.56
10	*26*	*0.88*	*0.41*	*1.65*	*119*	*4.03*	*80*	*2.71*
11	*43*	*1.16*	*0.4*	*1.69*	*260*	*8.80*	*37*	*5.01*
12	77	5.22	0.42	1.91	11	0.75	45	2.03
13	142	4.36	0.37	2.13	68	2.61	44	2.25
Mean ± SD	80 ± 50	3.2 ± 2.0	0.40 ± 0.02	1.8 ± 0.2	110 ± 90	3.7 ± 3.1	50 ± 17	2.7 ± 1.4

ADC, apparent diffusion coefficient; FA, fractional anisotropy; SD, standard deviation.
Volunteers number 10 and 11 written in italics are the ones with placental complication at second delivery.

out the surgical technique for performing a Caesarean section that will cause the least amount of fibre disruption in order to prevent future complications during subsequent deliveries.

Conclusion

The present study shows that 3 T MR-DTI can non-invasively depict the fibre architecture of the uterus *in vivo*. The newest applications propose diffusion spectrum imaging (DSI) as an evolution of DTI, which has a higher quality of angular resolution in 3D, particularly useful to visualise deeply crossed fibres, but it has a long sequence run time and it is not applicable *in vivo*. Recent animal studies analysed myocardium in rat hearts, bovine tongue and rat optic tracts with DTI and DSI, but at present hardware limitations hamper most of the clinical applications [19, 20]. It is hoped that as MR-DTI software and hardware improve and a uterine-specific fibre tracking algorithm is refined, we can expect a higher spatial resolution with decreased acquisition time. In future, MR-DTI will hopefully become a useful clinical tool to look for potential variation in uterine structure, especially in females with Caesarean scars, and improve the non-invasive view of uterine structure.

Acknowledgments

We thank all the volunteers who participated in this feasibility study and all the radiology technicians who gave their help and time in adjusting and performing the examinations, especially Paola Buffagni and Paola Trenti. Moreover, a special thanks to Henry Goodfellow, who helped us edit the paper.

References

1. Wetzstein R, Renn KH. Arrangement of smooth muscle in the human uterus. [In German.] Verh Anat Ges 1970;64: 461–8.
2. Hagmann P, Jonasson L, Maeder, Thiran JP, Wedeen VJ, Meuli R. Understanding Diffusion MR Imaging techniques: from scalar diffusion-weighted imaging to diffusion tensor imaging and beyond. Radiographics 2006;26:S205–23.
3. Mukherjee P, Berman JI, Chung SW, Hess CP, Henry RG. Diffusion tensor MR imaging and fibre tractography: theoretic underpinnings. AJNR Am J Neuroradiol 2008;29: 632–41.
4. Schaefer PW, Grant PE, Gonzales RG. Diffusion-weighted MR imaging of the brain. Radiology 2000;17:331–45.
5. Heemskerk AM, Strijkers GJ, Vilanova A, Drost MR, Nicolay K. Determination of mouse skeletal muscle architecture using three–dimensional diffusion tensor imaging. Magn Reson Med 2005;53:1333–40.
6. Gilbert RJ, Wedeen VJ, Magnusson LH, Benner T, Wang R, Dai G, et al. Three-dimensional myoarchitecture of the bovine tongue demonstrated by diffusion spectrum magnetic resonance imaging with tractography. Anat Rec A Discov Mol Cell Evol Biol 2006;288:1173–82.
7. Schmid P, Jaermann T, Boesiger P, Niederer PF, Lunkenheimer PP, Cryer CW, et al. Ventricular myocardial architecture as visualized in postmortem swine hearts using magnetic resonance diffusion tensor imaging. Eur J Cardiothoracic Surg 2005;27:468–72.
8. Lansdown DA, Ding Z, Wadington M, Hornberger JL, Damon BM. Quantitative diffusion tensor MRI-based fibre tracking of human skeletal muscle. J Appl Physiol 2007;103: 673–81.
9. Budzik JF, Le Thuc V, Demondion X, Morel M, Chechin D, Cotten A. In vivo MR tractography of thigh muscle using diffusion tensor imaging: initial results. Eur Radiol 2007;17: 3079–85.
10. Gaige TA, Benner T, Wang R, Wedeen VJ, Gilbert RJ. Three dimensional myoarchitecture of the human tongue determined in vivo by diffusion tensor imaging with tractography. J Magn Reson Imaging 2007;26:654–61.
11. Wu MT, Su MY, Huang YL, Chiou KR, Yang P, Pan HB, et al. Sequential changes of myocardial microstructure in patients postmyocardial infarction by diffusion-tensor cardiac MR: correlation with left ventricular structure and function. Circ Cardiovasc Imaging 2009;2:32–40.
12. Weiss S, Jaermann T, Schmid P, Staempfli P, Boesiger P, Niederer P, et al. Three-dimensional fibre architecture of the nonpregnant human uterus determined ex vivo using

magnetic resonance diffusion tensor imaging. Anat Rec A Discov Mol Cell Evol Biol 2006;288:84–90.
13. Martin JA, Hamilton BE, Sutton PD, Ventura SJ, Mathews TJ, Osterman MJ. Births: final data for 2008. Natl Vital Stat Rep 2010;59:1,3–71.
14. Usta IM, Hobeika EM, Musa AA, Gabriel GE, Nassar AH. Placenta previa-accreta: risk factors and complications. Am J Obset Gynecol 2005;193:1045–9.
15. Hager RM, Daltveit AK, Hofoss D, Nilsen ST, Kolaas T, Øian P, et al. Complications of cesarean deliveries: rates and risk factors. Am J Obstet Gynecol 2004;190:428–34.
16. Yao L, Gai N. Median nerve cross-sectional area and MRI diffusion characteristics: normative value at the carpal tunnel. Skeletal Radiol 2009;38:355–61.
17. Wu S, Kocherginsky M, Hibbard JU. Abnormal placentation: twenty-year analysis. Am J Obstet Gynecol 2005;192: 1458–61.
18. Makoha FW, Felimban HM, Fathuddien MA, Roomi F, Ghabra T. Multiple cesarean section morbidity. Int J Gynaecol Obstet 2004;87:227–324.
19. Sosnovik DE, Wang R, Dai G, Reese TG, Wedeen VJ. Diffusion MR tractography of the heart. J Cardiovasc Magn Reson 2009;11:47.
20. Gaige TA, Kwon HS, Dai G, Cabral VC, Wang R, Nam YS, et al. Multiscale structural analysis of mouse lingual myoarchitecture employing diffusion spectrum magnetic resonance imaging and multiphoton microscopy. J Biomed Opt 2008;13:064005.